Energy dissipation by whistler turbulence: Three-dimensional particle-in-cell simulations

Ouliang Chang, S. Peter Gary, and Joseph Wang

Citation: Physics of Plasmas (1994-present) **21**, 052305 (2014); doi: 10.1063/1.4875728
View online: http://dx.doi.org/10.1063/1.4875728
View Table of Contents: http://scitation.aip.org/content/aip/journal/pop/21/5?ver=pdfcov
Published by the AIP Publishing

Energy dissipation by whistler turbulence: Three-dimensional particle-in-cell simulations

Ouliang Chang,[1,a)] S. Peter Gary,[2,b)] and Joseph Wang[3,c)]
[1]*Oracle Corporation, Redwood City, California 94065, USA*
[2]*Space Science Institute, Boulder, Colorado, USA*
[3]*University of Southern California, Los Angeles, California, USA*

(Received 12 February 2014; accepted 28 April 2014; published online 12 May 2014)

Three-dimensional particle-in-cell simulations of whistler turbulence are carried out on a collisionless, homogeneous, magnetized plasma model. The simulations use an initial ensemble of relatively long wavelength whistler modes and follow the temporal evolution of the fluctuations as they cascade into a broadband, anisotropic, turbulent spectrum at shorter wavelengths. For relatively small levels of the initial fluctuation energy ϵ_e, linear collisionless damping provides most of the dissipation of the turbulence. But as ϵ_e and the total dissipation increase, linear damping becomes less important and, especially at $\beta_e \ll 1$, nonlinear processes become stronger. The PDFs and kurtoses of the magnetic field increments in the simulations suggest that intermittency in whistler turbulence generally increases with increasing ϵ_e and β_e. Correlation coefficient calculations imply that the current structure dissipation also increases with increasing ϵ_e and β_e, and that the nonlinear dissipation processes in these simulations are primarily associated with regions of localized current structures. [http://dx.doi.org/10.1063/1.4875728]

I. INTRODUCTION

An unsolved problem in plasma turbulence is the dissipation of fluctuation energy at short wavelengths. The dissipation of turbulence in neutral fluids is usually described in terms of a forward cascade to short wavelengths where collisional processes such as resistivity or viscosity convert fluctuating fluid energy into thermal energy. Turbulence in collisionless magnetized plasmas is also often described in terms of a forward cascade, although the processes which can contribute to dissipation at short wavelengths are much more diverse than in fluid turbulence. Such plasma dissipation processes include the linear damping of plasma modes (i.e., Landau and/or cyclotron damping[1]), various higher order dissipation processes (e.g., nonlinear Landau damping), and reconnection at current sheets in the plasma.[2]

This manuscript describes three-dimensional (3D) particle-in-cell (PIC) simulations of whistler turbulence with particular attention to fluctuating field dissipation. Recent PIC simulations[2,3] have begun with a large-scale sheared flow configuration subject to the Kelvin-Helmholtz instability; the consequent long-wavelength turbulence undergoes a forward cascade developing electron-scale current sheets which efficiently dissipate the fluctuation energy via associated parallel electric fields. Recent gyrokinetic kinetic Alfvén turbulence simulations[4] driven by an oscillating antenna also show current sheet formation at electron gyroradius scales and suggest that the current structures are damped collisionlessly by resonant wave-particle interactions.

In contrast, we here follow References 5–8 and begin with a collisionless, homogeneous, magnetized plasma upon which is imposed an initial ensemble of relatively long wavelength whistler fluctuations. At early times, the whistler modes undergo a forward cascade to a broadband, anisotropic, turbulent spectrum at shorter wavelengths. At later times, the field fluctuations are dissipated and the plasma electrons are heated, with a temperature anisotropy $T_\parallel > T_\perp$ where $\parallel$ and $\perp$ denote directions parallel and perpendicular, respectively, to the background magnetic field $\mathbf{B}_o = \hat{\mathbf{z}} B_o$. To study the physics of whistler turbulence dissipation as functions of the initial β_e and the initial fluctuation energy ϵ_e, where $\beta_e = 8\pi n_e k_B T_{\parallel e}/B_o^2$ and $\epsilon_e = \Sigma_{\mathbf{k}} |\delta \mathbf{B}|^2_{t=0}/8\pi n_e k_B T_{e,t=0}$, we organized simulation runs into two sets. In one set, we varied the initial $\beta_e = 0.01$, 0.1, 1.0 while fixing the initial fluctuation energy at $\epsilon_e = 2.0$; in the other set, we varied $\epsilon_e = 0.5$, 1.0, 2.0, 5.0 while fixing the initial $\beta_e = 0.1$. In certain diagnoses, we also include data from variable ϵ_e at three different β_e. All other plasma and computational parameters are the same as those in Ref. 6.

We determine the total dissipation rate Γ_{total} from the simulations by computing the overall rate of change of fluctuating magnetic and electric field energy densities:

$$\Gamma_{total} \equiv \frac{d[\delta B^2(t) + \delta E^2(t)]/8\pi K_{e,t=0}}{dt}, \tag{1}$$

where $\delta B^2(t) \equiv \Sigma_{\mathbf{k}} |\delta \mathbf{B}(\mathbf{k},t)|^2$ and $\delta E^2(t) \equiv \Sigma_{\mathbf{k}} |\delta \mathbf{E}(\mathbf{k},t)|^2$. The normalization factor is the initial electron kinetic energy density $K_{e,t=0}$. The instantaneous Γ_{total} can be calculated from the slope of the curve of total fluctuating energy time history shown in Fig. 1 of Ref. 7 and Fig. 1 of Ref. 6. A small smoothing factor is used to calculate Γ_{total}, i.e., an

a)ouliang@usc.edu.
b)pgary@lanl.gov.
c)josephjw@usc.edu.

average over every 6 electron plasma periods to reduce the noise.

We also define the linear damping rate of the fluctuating fields as Γ_{linear}. Linear theory assumes the fluctuation amplitude is sufficiently small that a normal mode of the plasma is proportional to $\exp(i\mathbf{k}\cdot\mathbf{x} - i\omega t)$ where $\omega = \omega_r + i\gamma$ so that $|\delta\mathbf{B}(\mathbf{k},t)|^2 = \delta B^2(\mathbf{k})\exp(2\gamma t)$ where γ is the imaginary part of the frequency computed from linear kinetic dispersion theory [e.g., Ref. 1] based on plasma conditions at t = 0. Therefore, the instantaneous Γ_{linear} can be approximated by an integral over all wavevectors $\mathbf{k}$:

$$\Gamma_{linear} \equiv \int_{\mathbf{k}} 2\gamma(\mathbf{k})[|\delta\mathbf{B}(\mathbf{k})|^2 + |\delta\mathbf{E}(\mathbf{k})|^2]d\mathbf{k}/8\pi K_{e,t=0}. \quad (2)$$

The integral is computed as $\Sigma_{\mathbf{k}} 2\gamma(\mathbf{k})[|\delta\mathbf{B}(\mathbf{k})|^2 + |\delta\mathbf{E}(\mathbf{k})|^2]/8\pi K_{e,t=0}$ on the computational grid.

The fluctuating magnetic field increment as a function of spatial separation length r is $\delta_{r_j}B_i = B_i(j+r) - B_i(j)$, and i and j are either x, y, or z. The kurtosis of magnetic field increments is then defined as $\langle \Im_{ij}^4 \rangle$:

$$\langle \Im_{ij}^4 \rangle \equiv \frac{\langle (\delta_{r_j}B_i)^4 \rangle}{\sigma_{ij}^4}, \quad (3)$$

where $\sigma_{ij} \equiv \langle |\delta_{r_j}B_i|^2 \rangle^{1/2}$ is the dimensional standard deviation and $\langle \cdots \rangle$ denotes an ensemble average over three dimensional space. A Gaussian distribution of field increments yields a kurtosis of 3; departures from a Gaussian distribution correspond to increasing values of the kurtosis and are a measure of what has been called turbulent intermittency.

The correlation coefficient of two quantities X and Y is denoted as

$$\rho(X,Y) = \frac{cov(X,Y)}{\sigma_X \sigma_Y}, \quad (4)$$

where cov denotes covariance, and σ is the standard deviation. The correlation coefficient is a normalized value between −1 and 1. Values close to 1 indicates that there is a positive linear relationship between X and Y, while values close to −1 indicate a negative linear relationship. Values close to or equal to 0 suggest there is no linear relationship between the two variables.

II. PARTICLE-IN-CELL SIMULATIONS

First, we quantify the fluctuating field energy dissipation contributed from linear damping and compare that against the total dissipation in the simulations. Figure 1 compares the total damping rate Γ_{total} (solid lines) versus the linear damping rate Γ_{linear} (dashed lines) for each of our simulations. The difference between the total and linear damping rates corresponds by definition to the dissipation due to nonlinear mechanisms which may come from various higher order wave-particle processes and/or reconnection. At early times of some cases, the linear damping rate computed from Eq. (2) is larger than the total dissipation rate computed from Eq. (1). A possible explanation for this unphysical result may be that the phases of the initial fluctuations in each simulation have been chosen at random and are therefore not fully self-consistent. We assume that nonlinear interactions eventually produce appropriate phase angles and yield a fully self-consistent ensemble of turbulent field fluctuations as the simulations evolve. We believe that the demonstration of clearly turbulent properties at late times in our simulations as described in our earlier papers, as well as the consistent result of $\Gamma_{linear} \leq \Gamma_{total}$ at late times in Figs. 1(a) and 1(b), support the appropriateness of this assumption.

Figure 1(a) illustrates the time histories of Γ_{total} and Γ_{linear} for three different values of β_e at $\epsilon_e = 2.0$. For this value of ϵ_e, linear damping accounts for most of the dissipation at both $\beta_e = 1.0$ and $\beta_e = 0.10$, whereas nonlinear processes clearly dominate Γ_{total} at $\beta_e = 0.01$.

Figure 1(b) shows the time histories of Γ_{total} and Γ_{linear} for four different values of ϵ_e at $\beta_e = 0.1$. For this value of β_e, it is clear that the nonlinear processes contribute a monotonically increasing percentage of the total dissipation as the initial fluctuation energy increases.

Figure 1(c) compares Γ_{total} and Γ_{linear} as functions of both ϵ_e and β_e at relatively early times. For each value of β_e, the ratio $\Gamma_{linear}/\Gamma_{total}$ diminishes as ϵ_e increases, indicating the increasing importance of nonlinear processes. In contrast, for fixed ϵ_e, $\Gamma_{linear}/\Gamma_{total}$ increases as β_e becomes larger, consistent with the prediction of linear theory that damping of whistler fluctuations monotonically increases with increasing β_e, as in Fig. 8 of Ref. 6. For example, at $\epsilon_e = 5.0$, for $\beta_e = 0.01$, $\Gamma_{linear}/\Gamma_{total} \simeq 2\%$; for $\beta_e = 0.1$, $\Gamma_{linear}/\Gamma_{total} \simeq 50\%$; and for $\beta_e = 1.0$, $\Gamma_{linear}/\Gamma_{total} \simeq 77\%$. In summary, for relatively small levels of the initial fluctuation energy, linear collisionless damping provides most of the turbulent dissipation. But as ϵ_e and the total dissipation increase, linear damping becomes less important and, especially at $\beta_e \ll 1$, nonlinear processes become stronger.

We next investigate intermittency in our simulations. Intermittency can be framed in terms of the probability density function (PDF) of the fluctuating magnetic field increments δ_{rjB_i} as functions of spatial separation length r with greater departures from a Gaussian distribution corresponding to a more intermittent ensemble of fluctuations. Figure 2 shows the normalized PDFs for $r_y = 0.1\lambda_e$, $1\lambda_e$, $2.5\lambda_e$, $5\lambda_e$, $10\lambda_e$, $25\lambda_e$ as labeled from the $\beta_e = 0.1$ and $\epsilon_e = 2.0$ simulation at $|\Omega_e|t = 134.2$, where $\lambda_e = c/\omega_e$ is the electron inertial length, ω_e is the electron plasma frequency, and Ω_e is the electron cyclotron frequency. Panel (a) illustrates PDFs for one of the perpendicular magnetic field increments $\delta_{ry}B_x$ whereas Panel (b) illustrates PDFs for the parallel magnetic field increments $\delta_{ry}B_x$. As the spatial separation r_y is decreased, both PDFs become increasingly non-Gaussian, especially in the tails of the PDFs. However, there is a noticeable anisotropy between the PDFs of the perpendicular and parallel field increments. PDFs of $\delta_{ry}B_x$ have much larger non-Gaussian tails than those of $\delta_{ry}B_x$, indicating stronger intermittency in the $\delta B_\parallel$ component. This anisotropy could be explained by the fact that whistler turbulence cascades lead to strongly oblique propagation, which results in more contribution from $\delta B_\parallel$ than $\delta B_\perp$ in the probability

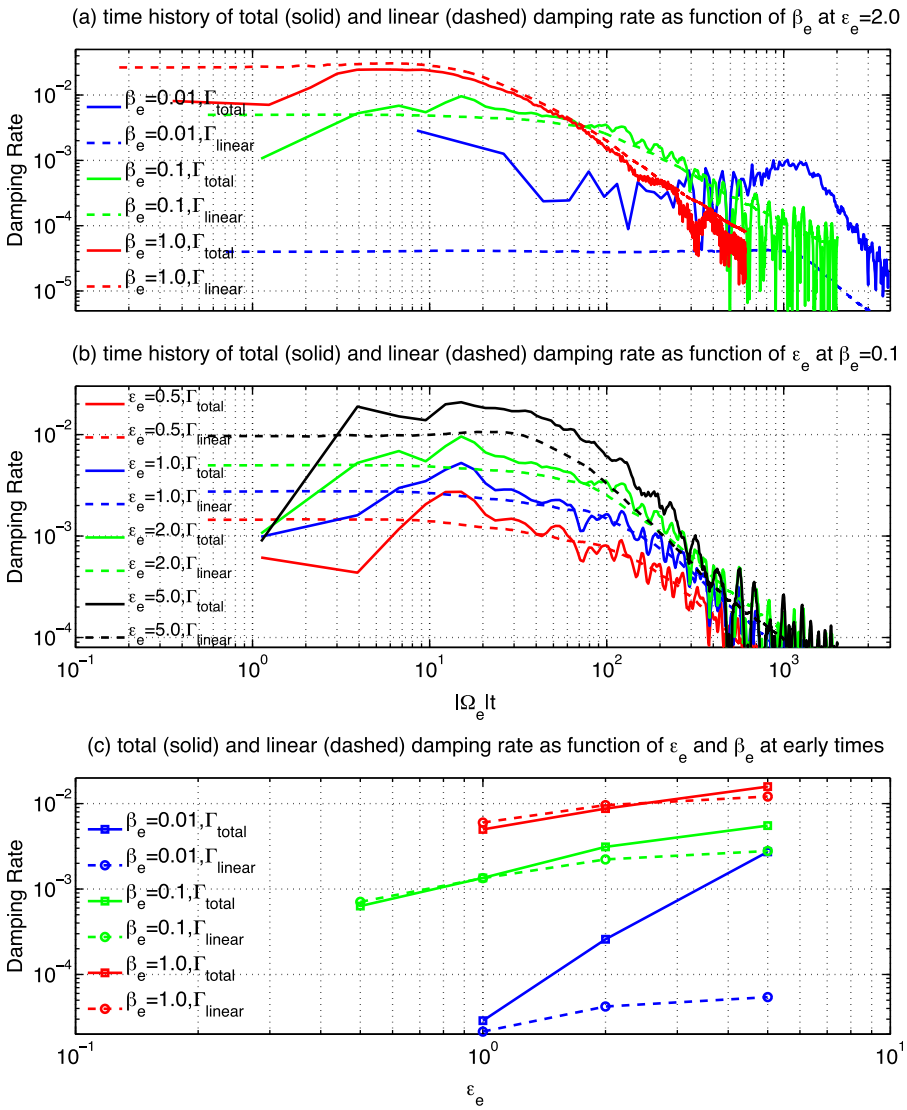

FIG. 1. Comparison of total damping rate Γ_{total} (solid lines) and linear damping rate Γ_{linear} (dashed lines) (a) as functions of β_e and $|\Omega_e|t$ at $\epsilon_e = 2.0$; (b) as functions of ϵ_e and $|\Omega_e|t$ at $\beta_e = 0.1$; (c) as functions of ϵ_e and β_e at their respective early times, that is for $\beta_e = 0.01$ cases, $|\Omega_e|t = 707.1$; for $\beta_e = 0.1$ cases, $|\Omega_e|t = 111.8$; and for $\beta_e = 1.0$ cases, $|\Omega_e|t = 35.4$.

density function calculation. Reference 9 finds that the PDFs of $\delta_r B_\perp$ and $\delta_r B_\parallel$ are similar for kinetic Alfvén waves. Therefore, this difference might help in distinguishing between whistlers and kinetic Alfvén waves in short-wavelength turbulence.

The PDFs in Figure 2 have enhanced tails at large increments, but fit well to Gaussians at small increments. This is in contrast to the PDFs of Refs. 2, 9, and 10, which show strong departures from Gaussians at both large and small increments. We believe that the enhanced PDF tails are due to the intermittency in short-wavelength turbulence, but that the steepening of the PDFs at small increments is due to the presence of large-scale inhomogeneities. When summing over Gaussians with somewhat different standard deviations, a so-called Castaing distribution is formed, which usually has a more peaked distribution at small increments.[11] This implies that observations[9] and simulated turbulence driven by long-wavelength instabilities[2] may sum over many different small-scale measurements in inhomogeneous plasmas, so that their PDFs represent several different local Gaussians which result in the more peaked distributions at small increments, whereas Figure 2's relatively Gaussian PDFs at small increments confirms that our simulations are carried out on a homogeneous medium. Similar PDF characteristics with non-Gaussian tails but Gaussian-like shapes at small increments are reported in Refs. 12 and 13.

Another quantity which can be an indicator of intermittency and current structures is kurtosis as defined in Eq. (3). Figure 3 shows results for several different values of ϵ_e for three cases: the kurtoses of $\delta_{rx}B_z$ as functions of r_x at $\beta_e = 0.01$; the kurtoses of $\delta_{rz}B_y$ as functions of r_z at $\beta_e = 0.10$; and the kurtoses of $\delta_{ry}B_z$ as functions of r_y at $\beta_e = 1.0$. In most cases, the kurtosis grows from near-Gaussian values at scales larger than $10\lambda_e$ to strongly non-Gaussian values near and below electron scales $\leq \lambda_e$. The kurtosis increases with increasing ϵ_e and β_e and also generally increases with decreasing spatial separation length r until reaching constant values at $r < \lambda_e$. This behavior clearly signifies the statistical intermittency of the turbulence which shows the same trend as the current and electron pressure correlation coefficient $\rho(n_e T_e, J^2)$ in Table I. The noticeable jump of the kurtosis values near $\sim k\lambda_e$ between $\epsilon_e = 5.0$ cases and other lower ϵ_e cases at $\beta_e = 0.01$ and 0.1 indicates the point when intermittent current structures become relatively dominant in these whistler turbulence simulations. Note that the kurtosis values in our simulations are much smaller than those in the recent large-scale

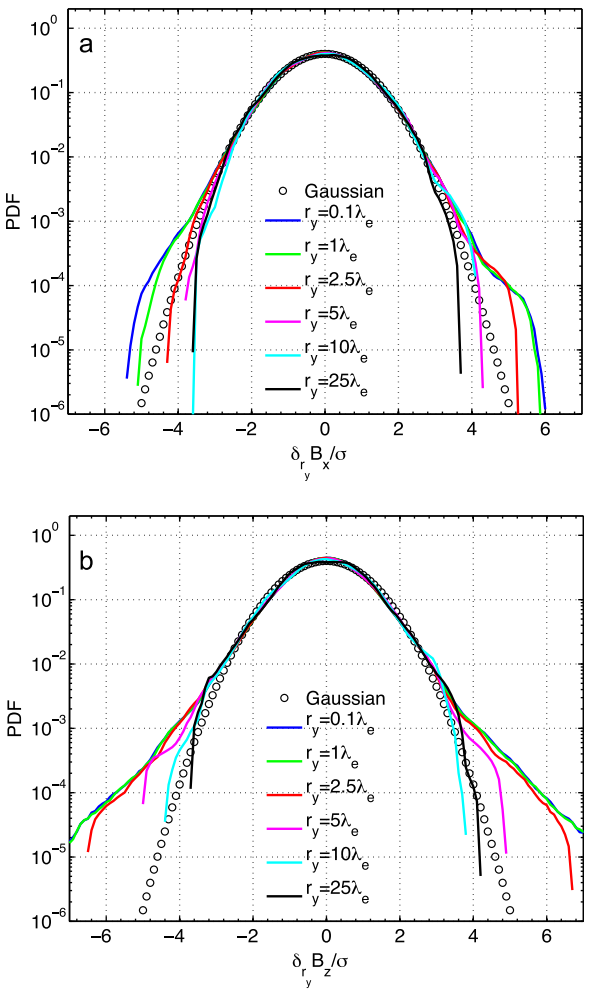

FIG. 2. Normalized PDFs of fluctuating magnetic field increments from the simulation starting with $\beta_e = 0.1$ and $\epsilon_e = 2.0$ at $|\Omega_e|t = 134.2$ for different spatial separation lengths r as labeled. (a) A perpendicular component $\delta_{ry}B_x$; (b) the parallel component $\delta_{ry}B_z$. Here, the PDFs are normalized to the standard deviation σ of their respective magnetic field increments. The black circled lines indicate Gaussian distributions.

two-dimensional (2D) PIC simulation of sheared-flow-driven turbulence[3] which yields values up to 10.5. This indicates again that our simulations remain relatively homogeneous.

TABLE I. Correlation coefficients between n_eT_e and J^2. All grid points in the 3D simulation space are taken into account.

$\rho(n_eT_e, J^2)$	$\beta_e = 0.01$	$\beta_e = 0.1$	$\beta_e = 1.0$
$\epsilon_e = 1.0$	0.138	0.245	0.326
$\epsilon_e = 2.0$	0.219	0.304	0.336
$\epsilon_e = 5.0$	0.247	0.368	0.412

We also examined whether current structures are formed in our simulations by plotting parallel current density $J_\parallel$ in a x-y plane with spatial band-pass filters applied in a similar fashion as in Fig. 2 of Ref. 4. These figures in Ref. 7 (Figs. 6.2–6.4) suggest that current structures form primarily at $|k_\perp \lambda_e| \geq 1$ for all three $\beta_e = 0.01$, 0.1, and 1.0 runs. The current structures in our simulations form self-consistently from the cascade of decaying turbulence without any driving force and are not seeded or otherwise initialized. Therefore, we conclude that electron-scale current structures form as a natural consequence of whistler turbulence, even in weakly perturbed, relatively homogeneous plasmas such as these 3D PIC simulations.

To investigate the relationship between energy dissipation associated with current structures and the total electron heating measured in the simulation, we compute the correlation coefficient, $\rho(n_eT_e, J^2)$, between the current density squared J^2 and the electron pressure n_eT_e in the simulations as functions of both β_e and ϵ_e. The values are listed in Table I. Note that, in general, $\rho(n_eT_e, J^2)$ does not reflect Landau/cyclotron damping's correlation with electron pressure. The current density J on its own does not necessarily correspond to Landau damping, because in the micropicture, J means a velocity shift of all the electrons relative to the ions.

Table I shows that an increase in the initial fluctuation energy density translates into a monotonic increase in the coefficient $\rho(n_eT_e, J^2)$. The increasing correlation between current density and electron pressure with increasing ϵ_e is consistent with the hypothesis that nonlinear processes in whistler turbulence play increasing roles in energy dissipation with increasing ϵ_e as shown in Figure 1(c). Furthermore,

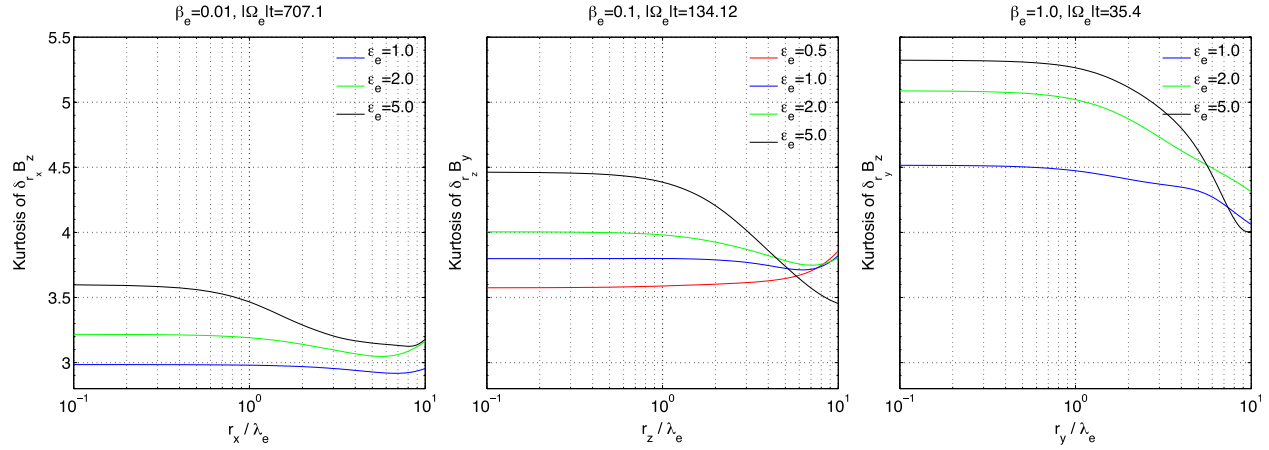

FIG. 3. Kurtoses of the magnetic field increments δ_{rjB_i} as functions of spatial separation length r for different ϵ_e and β_e as labeled. The left panel is from $\beta_e = 0.01$ cases at $|\Omega_e|t = 707.1$; the middle panel is from $\beta_e = 0.1$ cases at $|\Omega_e|t = 134.12$; and the right panel is from $\beta_e = 1.0$ cases at $|\Omega_e|t = 35.4$. Data are low pass filtered at $k_{x/y/z}\lambda_e = 5$ to remove the statistical noise due to finite superparticle number in the PIC simulations.

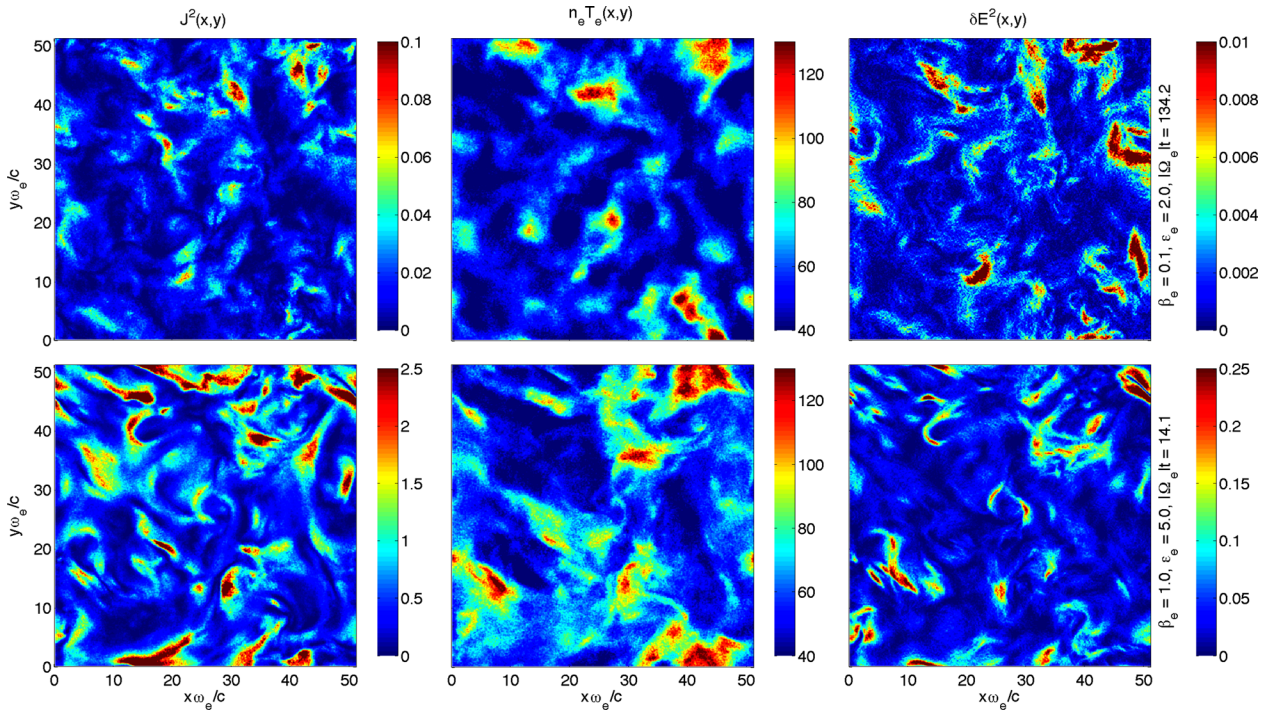

FIG. 4. Current density squared J^2 (left column), electron pressure n_eT_e (middle column), and electric field energy δE^2 (right column) from a perpendicular plane $(x-y)$. The color contours represent normalized simulation values of corresponding quantities. The upper panels are from the $\beta_e = 0.1$ and $\epsilon_e = 2.0$ case at $|\Omega_e|t = 134.2$, and the correlation coefficient ratio $\frac{\rho(n_eT_e,J^2)}{\rho(n_eT_e,\delta E^2)} = 4.83$. The lower panels are from $\beta_e = 1.0$ and $\epsilon_e = 5.0$ case at $|\Omega_e|t = 14.1$, and the correlation coefficient ratio $\frac{\rho(n_eT_e,J^2)}{\rho(n_eT_e,\delta E^2)} = 1.92$. Note that the correlation coefficients are computed from all grid points in the 3D space, not just the 2D planes shown here.

this correlation coefficient increases with increasing β_e. In the limit of zero β_e, the magnetic field is rigid and there are no current sheets. As β_e increases, the magnetic field becomes weaker and the plasma currents act to change the magnetic field, forming current structures. Therefore, current structure formation and dissipation should increase with increasing β_e, at least for $\beta_e \lesssim 1$.

Figure 4 shows the spatial contours of J^2, n_eT_e and δE^2 from two typical cases, that is, the upper panels represent $\beta_e = 0.1$ and $\epsilon_e = 2.0$ case at $|\Omega_e|t = 134.2$, and the lower panels represent $\beta_e = 1.0$ and $\epsilon_e = 5.0$ case at $|\Omega_e|t = 14.1$. The relatively strong correlation between J^2 and n_eT_e indicates that current structure formation is playing an important role in whistler turbulence simulations here. The spatial structures of J^2 resemble the electron pressure n_eT_e structures shown in Figure 4, providing a qualitative evidence of dissipation in regions of coherent intermittent structures.

The relative contribution to electron heating from linear damping could be studied by calculating the coefficient $\rho(n_eT_e, \delta E^2)$. For Landau/cyclotron damping to be involved, there must be a microscopic quantity involved, such as δE_z or δE. We note that $\rho(n_eT_e, \delta E^2)$ does not uniquely represent the correlation between linear damping and electron heating, but just involves linear dissipation effects. The correlation coefficient ratio $\frac{\rho(n_eT_e,J^2)}{\rho(n_eT_e,\delta E^2)}$ implies the relative contribution between current structure dissipation and linear damping. In Figure 4, the ratio from $\beta_e = 0.1$ case is 4.85, whereas $\frac{\rho(n_eT_e,J^2)}{\rho(n_eT_e,\delta E^2)}$ from $\beta_e = 1.0$ case is 1.92, as listed in Table II. The ratio in Table II decreases with increasing β_e, indicating the relatively smaller importance of current structure dissipation and greater importance of linear damping in higher β_e plasmas, and this trend is consistent with that of Figure 1(c). Therefore, the decreasing ratio $\frac{\rho(n_eT_e,J^2)}{\rho(n_eT_e,\delta E^2)}$ with increasing ϵ_e and β_e indicates that the relative contribution between current structure dissipation and linear damping is ultimately determined by β_e rather than ϵ_e, and is a weak function of ϵ_e.

TABLE II. Correlation coefficient ratios $\frac{\rho(n_eT_e,J^2)}{\rho(n_eT_e,\delta E^2)}$. All grid points in the 3D simulation space are taken into account.

$\frac{\rho(n_eT_e,J^2)}{\rho(n_eT_e,\delta E^2)}$	$\beta_e = 0.1$	$\beta_e = 1.0$
$\epsilon_e = 2.0$	4.85	1.85
$\epsilon_e = 5.0$	6.75	1.92

III. CONCLUSIONS

Using results from the three-dimensional PIC simulations of Refs. 6 and 8 we have for the first time examined dissipation properties of the forward cascade of homogeneous whistler turbulence in a collisionless, magnetized plasma. By computing the ratio of dissipation rates $\Gamma_{linear}/\Gamma_{total}$, we find that linear damping constitutes the majority of the total dissipation at sufficiently small initial amplitudes, that nonlinear processes increase in relative importance as ϵ_e increases, and that for fixed ϵ_e linear damping increases as β_e becomes larger, consistent with the predictions of linear dispersion theory. These conclusions are consistent with the strongly driven results of Ref. 2, who found current sheet heating to be several orders of magnitude more efficient than damping by kinetic Alfven waves, and with the less strongly driven results of Ref. 4, who concluded that

collisionless damping of kinetic Alfven waves is sufficient to account for all of the heating in their simulations. Reference 2 indicates that electron heating from reconnection should be parallel to $\mathbf{B}_o$ and scale as $1/\beta_e^{1/2}$. Our PIC simulations show that electron heating from whistler turbulence is also primarily parallel to $\mathbf{B}_o$ [*Gary et al.*, 2012, Fig. 1(b), and *Chang et al.*, 2013, Fig. 4(b)] and that this parallel heating scales as a weaker inverse power of β_e. So there is a consistent trend between the electron heating results of our simulations and those of Ref. 2, although this consistency does not necessarily demonstrate that reconnection plays a role in whistler turbulence.

We further quantify the intermittency in our simulations by showing that the PDFs of magnetic field increments depart more strongly from Gaussian distributions as the separation length decreases. The PDFs at short spatial separations are anisotropic between $\delta_{r\mathbf{B}\perp}$ and $\delta_r B_\parallel$ with the latter having much larger values in the tails of the distribution, which is probably due to the strongly oblique propagation induced by the whistler cascade. The kurtosis of the magnetic field increments similarly increases from the value of three, corresponding to a Gaussian PDF at much larger than electron scales, to non-Gaussian values ranging from $3.5 \sim 5.5$ near and below electron scale lengths. Furthermore, the kurtosis in whistler turbulence generally increases with increasing ϵ_e and β_e.

The correlation coefficient $\rho(n_eT_e, J^2)$ shows monotonic increases as either ϵ_e or β_e increase, showing that current structure dissipation is positively correlated with both of these parameters. We estimate the relative contribution to the overall electron heating from current dissipation and linear damping by computing the correlation coefficient ratio $\frac{\rho(n_eT_e,J^2)}{\rho(n_eT_e,\delta E^2)}$. The ratio decreases with increasing β_e, implying a lesser importance of current dissipation and a greater importance of linear damping in higher β_e plasmas. Because the relative contribution from linear damping generally increases with β_e and decreases with ϵ_e, the decreasing ratio $\frac{\rho(n_eT_e,J^2)}{\rho(n_eT_e,\delta E^2)}$ with increasing β_e and ϵ_e also suggests that the relative contribution between current structure dissipation and linear damping is ultimately determined by β_e rather than ϵ_e. These properties maintain a consistent correlation with the trends of the relative contributions from linear and nonlinear dissipation described in Figure 1. Therefore, we conclude that the nonlinear dissipation processes involved in whistler turbulence are primarily at current structures.

ACKNOWLEDGMENTS

The authors acknowledge useful exchanges with Jason TenBarge. S.P.G.'s contributions to this research were supported by the Heliophysics Guest Investigators Program of the National Aeronautics and Space Administration (NASA), Grant No. NNX12AJ96G and by the joint DOE/National Science Foundation program in fundamental plasma research. The USC portion of this work was supported by the National Science Foundation Grant No. AGS-1202603. Computational resources supporting this work were provided by the NASA High-End Computing (HEC) Program through the NASA Advanced Supercomputing (NAS) Division at Ames Research Center as well as by the Yellowstone supercomputer provided by National Center for Atmospheric Research (NCAR)'s Computational and Information Systems Laboratory (CISL) sponsored by the National Science Foundation.

[1]S. P. Gary, *Theory of Space Plasma Microinstabilities* (Cambridge University Press, New York, 1993).
[2]H. Karimabadi, V. Roytershteyn, M. Wan, W. H. Matthaeus, W. Daughton, P. Wu, M. Shay, B. Loring, J. Borovsky, E. Leonardis, S. C. Chapman, and T. K. M. Nakamura, Phys. Plasmas **20**, 012303 (2013).
[3]M. Wan, W. H. Matthaeus, H. Karimabadi, V. Roytershteyn, M. Shay, P. Wu, W. Daughton, B. Loring, and S. C. Chapman, Phys. Rev. Lett. **109**, 195001 (2012).
[4]J. M. TenBarge and G. G. Howes, Astrophys. J. **771**, L27 (2013).
[5]O. Chang, S. P. Gary, and J. Wang, Geophys. Res. Lett. **38**, L22102, doi:10.1029/2011GL049827 (2011).
[6]O. Chang, S. P. Gary, and J. Wang, J. Geophys. Res. **118**, 2824, doi:10.1002/jgra.50365 (2013).
[7]O. Chang, "Three-dimensional kinetic simulations of whistler turbulence in solar wind on parallel supercomputers," Ph.D. dissertation (University of Southern California, 2013).
[8]S. P. Gary, O. Chang, and J. Wang, Astrophys. J. **755**, 142 (2012).
[9]K. H. Kiyani, S. C. Chapman, F. Sahraoui, B. Hnat, O. Fauvarque, and Yu. V. Khotyaintsev, Astrophys. J. **763**, 10 (2013).
[10]K. T. Osman, W. H. Matthaeus, M. Wan, and A. F. Rappazzo, Phys. Rev. Lett. **108**, 261102 (2012).
[11]L. Sorriso-Valvo, V. Carbone, P. Veltri, G. Consolini, and R. Bruno, Geophys. Res. Lett. **26**, 1801, doi:10.1029/1999GL900270 (1999).
[12]D. Perrone, F. Valentini, S. Servidio, S. Dalena, and P. Veltri, Astrophys. J. **762**, 99 (2013).
[13]J. He, C. Tu, E. Marsch, S. Bourouaine, and Z. Pei, Astrophys. J. **773**, 72 (2013).